Published in final edited form as:
Microsc Res Tech. 2012 March ; 75(3): 300–306. doi:10.1002/jemt.21058.

Anisotropic Properties of Bovine Nasal Cartilage

Yang Xia, PhD[*], **Shaokuan Zheng, PhD**[1], **Matthew Szarko, PhD**[2], and **Jihyun Lee, BSc**
Department of Physics and Center for Biomedical Research, Oakland University, Rochester, MI 48309, USA

Abstract

To investigate the structural anisotropy in bovine septal cartilage, quantitative procedures in microscopic magnetic resonance imaging (μMRI), polarized light microscopy (PLM), and mechanical indentation were used to measure the tissue in three orthogonal planes: vertical, medial, and caudocephalic. The quantitative T2 imaging experiments in μMRI found strong anisotropy in the images of both vertical and caudocephalic planes but little anisotropy in the images from the medial plane. The PLM birefrigent experiments found that the retardation values in the medial section were only about 10% of these in the vertical and caudocephalic sections and that the angle values in all three sections followed the rotation of the tissue section in the microscope stage. The stress relaxation experiments in mechanical indentation showed reduced stiffness in the medial plane compared to stiffness in either the vertical or caudocephalic planes. Collectively, the results in this project coherently indicate a marked structural anisotropy in cartilage from the nasal septum, where the long axis of the collagen fibrils is oriented in parallel with the medial axis.

Keywords

bovine nasal cartilage; collagen anisotropy; MRI; PLM; biomechanical indentation

Introduction

As a transplant material, cartilage is used extensively in reconstructive surgery (e.g. facial and orthopaedic surgery) (Glasgold and others, 1988; Grellmann and others, 2006; Rotter and others, 2002), as it can easily be carved to fit the desired contour (Maas and others, 1998). It can be procured in abundance from the patient, from other individuals as homografts removed during routine surgery, or from cadaveric donor tissue (Donald, 1986). Of the various cartilages in the human body, septal cartilage is commonly used as an ideal support and filler material, owing to the large amount of collagen-based intercellular substance (Cardenas-Camarena and others, 1998). The organization of the extracellular matrix in cartilage, chiefly comprised of collagen and proteoglycans, can affect the physical properties of the tissue (Arokoski and others, 1993; Jeffery and others, 1991; Muir and others, 1970). Many cartilage grafts experience post-surgical resorption, the greatest disadvantage of cartilage as a transplant material (Donald, 1986). Resorption rates of septal cartilage grafts have been estimated as ranging from 12-50% (Maas and others, 1998). Septal cartilage resorption following surgical implantation may result from extracellular anisotropies within cartilage (Grellmann and others, 2006). (Anisotropy refers to the

[*]Corresponding Author and Address: Yang Xia, PhD, Department of Physics and Center for Biomedical Research, Oakland University, Rochester, Michigan 48309, USA, Phone: (248) 370-3420, Fax: (248) 370-3408, xia@oakland.edu.
[1]Present Address: Department of Radiology, Univ. of Massachusetts Medical School, Worcester, MA 01655, USA.
[2]Present Address: Division of Biomedical Sciences, St. George's, University of London, London, SW17 0RE, UK.

property of the material being directionally dependent.) The post-surgical importance of extracellular anisotropies is not unique to septal cartilage. Malrotation of articular cartilage grafts, with respect to superficial collagen orientation (split-lines), has been suggested to change the tensile resistance properties of superficial articular cartilage and potentially lead to diminished articular graft longevity (Bisson and others, 2005). Improved understanding of extracellular anisotropy of septal cartilage may prove to be important for understanding the host-graft relationship and the potential for graft resorption.

The similarities between the extracellular macromolecules have also allowed septal cartilage to frequently be used as a substitute in studies of articular cartilage by the NMR/MRI (Jelicks and others, 1993; Reiter and others, 2009; Zheng and Xia, 2009a; b; 2010a; b; Zheng and others, 2009). In these studies however, little attention is paid to the structural orientation of the tissue, as septal cartilage is generally assumed to be isotropic. Collagen anisotropy within articular cartilage has been associated with the depth-dependent physical properties of the tissue (Xia, 2008; Xia and others, 2007; Xia and others, 2008). The existence of any collagen anisotropies in septal cartilage, to the best of our knowledge, has only been observed in a compressive biomechanical study of human tissue (Richmon and others, 2006). The current investigation studied septal cartilage in three orthogonal planes, where the normal axes were in parallel with the vertical, medial, and caudocephalic axes respectively (Fig 1a), using not only mechanical indentation but also two microscopic imaging techniques (microscopic magnetic resonance imaging (μMRI), and polarized light microscopy (PLM)). We aimed to identify the potential linkages between the mechanical anisotropy with the anisotropies of collagen within the septal tissue, which may play an important role in post-surgical resorption of septal grafts.

Materials and Methods

Bovine Nasal Cartilage Samples

Cartilage from bovine nasal septa, harvested fresh from a local slaughterhouse, was immersed in saline (154 mM NaCl in deionized water) and kept at -20 °C before experimental measurements. For μMRI and PLM imaging experiments, a total of twelve tissue blocks were obtained from the central region of the septal cartilage along three orthogonal directions, four blocks for each orthogonal direction (Fig 1). All tissue blocks had the same physical dimension, ~ 1.5 mm × 1.5 mm × 5 mm. Each tissue block had sides parallel to three orthogonal planes, where the normal axes of these planes were in parallel with the vertical, medial (left/right), and caudocephalic axes respectively (Fig 1). (The 2D planes/surfaces/images studied are being referred to as the vertical, medial, and caudocephalic planes/surfaces/images in this report.) In addition, two long strips of tissue were obtained from the adjacent regions of the imaging specimens, in the same orientational manner, for mechanical testing.

Microscopic MRI (μMRI) Method

The μMRI experiments were performed at room temperature (about 20°C) on a Bruker AVANCE II 300 NMR spectrometer equipped with a 7-Tesla/89-mm vertical-bore superconducting magnet and micro-imaging accessory (Bruker Instrument, Billerica, MA). A homemade 4-mm solenoid coil, which includes a rotation device, was used in the μMRI experiments (Xia and others, 2002). Each tissue block was imaged thirteen times, using the identical imaging parameters, except the physical orientation of the block was rotated inside the magnet over a range of 180°, at an interval of 15° (θ in Fig 1c) with respect to the direction of $\mathbf{B}_0$. The rotation axis, in parallel with the long axis of the cartilage block, remained unchanged and perpendicular to the static magnetic field ($\mathbf{B}_0$) during the experiments (Fig 1c). At each orientation, a quantitative T_2 imaging experiment was

performed using a CPMG magnetization-prepared T_2 imaging sequence (Zheng and Xia, 2009b), which allows an accurate measurement of the tissue T_2. All μMRI images were obtained from an identical 2D image slice location, approximately in the middle of the tissue block (Fig 1c). The echo spacing in the CPMG T_2-weighting segment was 1 ms, and the number of echoes were 2, 80, 200, 400, which corresponded to four echo delays of 2, 80, 200, 400 ms respectively for the four T_2-weighted images in the experiments. Other imaging parameters included: a 7.2 ms echo time in the imaging segment; a 3.2 × 3.2 mm^2 field of view; a 64 × 64 imaging matrix size; a 50 kHz spectral bandwidth, corresponding to a readout sampling dwell time of 20 μs; 0.8 ms and 0.507 ms hermite-shape pulses were used as excitation and refocusing pulses in the imaging segment, respectively; and a 2 second repetition time (TR) in the imaging experiment. From the average intensity in the central part of each T_2-weighted image, the T_2 relaxation in cartilage was calculated by a single exponential fitting of the data, which assumes that there is only one T_2 component in bovine septal cartilage (Zheng and Xia, 2009b; 2010a). The transverse resolution in imaging was 50 × 50 μm and the slice thickness was 1mm.

Polarized Light Microscopy (PLM) method

After the non-destructive μMRI experiments, the same tissue blocks were embedded in the deionized water medium and cryo-sectioned to 6 μm thickness along the three orthogonal planes (Fig 1d) resulting in three types of thin tissue sections: vertical sections, medial sections, and caudocephalic sections. A total of 90 thin sections were made from these tissue blocks. These tissue sections were placed on mirrIR slides (Kevley Technologies, Chesterland, OH) and imaged using a Leica polarizing light microscope fitted with a commercial imaging system (Cambridge Research & Instrumentation, Woburn, MA). Each tissue section was imaged nine times under the identical parameters and conditions, except each time with a 15°-30° rotation of the tissue section on the microscope stage. A 5× objective was used in the PLM imaging experiments, which yielded a pixel size of 2.0 μm.

From this PLM procedure, each imaging experiment generates two quantitative 2D images, one retardation image (in unit of nm) and one angle image (in unit of degree) (Xia and others, 2001). Based on the physical mechanism of birefringence, the angle maps in this PLM procedure illustrate the averaged orientations of the collagen fibrils in each pixel of the tissue, whereas the retardance maps are influenced by several factors in the experiment, including the randomness of the collagen fibrils, the fibril diameter, the packing density of the fibrils, and the thickness of the tissue section. For any single tissue section, a smaller retardance value indicates that the collagen fibrils are less ordered (Xia and others, 2003; Xia and others, 2001).

Biomechanical Protocols

A total of 11 tissue blocks were obtained one at a time from the two long strips of tissue. Each block was about 3 mm × 3 mm × 3 mm in physical dimension, and trimmed of medial nasal mucosa to expose the underlying septal cartilage for mechanical testing. Different surfaces of the tissue block were identified using colored inks that were applied outside of the contact area after the testing of each surface. The sample was placed in a rectangular aluminum box that was attached to a multi-axial rotational table vise, which allowed precise sample positioning that ensured perpendicularity between the cartilage surface and the indenter. The aluminum box was larger than the sample so that the specimen was not constrained in any way. Sample dehydration was prevented by sample exposure to saline throughout testing. Each sample was loaded in this manner in each of the three orthogonal planes mentioned previously. A semi-spherical indenter (2 mm diameter) attached to the actuator of an Enduratec ELF 3200 material test system (Bose Corporation, Eden Prairie, MN) compressed the sample to a maximum load of 0.1N. This level of compression was

held for 5 minutes and the relaxation behavior of the tissue was recorded (820 sampling points).

Results

Microscopic MRI results

Fig 2 shows a representative set of the proton intensity image and the calculated T_2 image, from one specimen at one orientation. It is clear that the intensity and T_2 images in septal cartilage are relatively homogeneous (i.e., lack of the zonal features in articular cartilage (Xia and others, 2001)). However, when the T_2 values at the same location of all thirteen T_2 images from the same specimen were extracted, the tissue anisotropy was identified from the T_2 anisotropy profile plots. Fig 3 shows the experimental results of R_2 ($1/T_2$) relaxation rate from a set of septal cartilage blocks during the specimen rotation experiments, where each tissue block was rotated around its long axis (Fig 1c). A distinct difference can be seen in the T_2 relaxation characteristics between the rotation of Block Y and Blocks X/Z: the T_2 characteristics in both Block X (images in the caudocephalic plane) and Block Z (images in the vertical plane) are highly anisotropic (Fig 3a and 3b), while the T_2 characteristics in Block Y (images in the medial plane) are isotropic (Fig 3c). These experimental results indicate the averaged orientation of the collagen fibrils in the septal cartilage is in parallel with the medial direction of the anatomic structure of septum (Fig 1a).

The imaging data in Fig 3 were also fitted with a fibril model (Zheng and Xia, 2009c; Zheng and others, 2011). A fibril bundle with little divergence was found to best fit the experimental data when the rotational axis was oriented along either vertical or caudocephalic directions (Fig 3a and 3b). When the rotational axis was oriented along the medial direction, a constant R_2 value was observed (Fig 3c), which indicated the approximate parallelism between the rotational axis and the direction of the fibril bundle in Block Y, again in parallel with the medial direction of the anatomic structure of the septum.

PLM results

The quantitative images of the tissue angle and retardation from PLM also showed the collagen anisotropy in septal cartilage (Fig 4). The angle and retardation maps from the vertical and caudocephalic sections (Fig 1d) showed similar birefringent patterns, where the images appeared to show a view along the length of the collagen fibrils that accommodated the chondrocytes (Fig 4). In contrast, the angle and retardation maps from specimens sectioned in the medial plane were very different and appeared to show an end view of the collagen fibrils (Fig 4).

Each sample was imaged nine times at different orientations. The values in these quantitative images (taken from approximately the same location within the images) were extracted and plotted as a function of the tissue orientation on the microscope stage in Fig 5. Fig 5a shows no anisotropy in the retardation values. However, the values of the retardation in the samples sectioned in the medial plane were about 10% of the values from samples sectioned in either vertical or caudocephalic planes. This indicates a significantly decreased fibril order in the medial plane when compared to either vertical or caudocephalic planes. The angle values in Fig 5b show strong anisotropy in all orthogonal planes. Since each set of the angle values on this plot came from nine sets of PLM images where each image was obtained when the tissue section was rotated to a different physical orientation on the microscope stage, a linear relationship between the specimen rotation and the measured angle value is a clear indication that there is a collagen anisotropy in these thin tissue sections.

Biomechanical Results

Biomechanical results also show substantial anisotropy in the compressive properties of the septal cartilage samples, shown in Fig 6 as the averaged relaxation characteristics of the specimens. The stress relaxation profiles of the various orthogonal planes show very similar relaxation behavior for both the caudocephalic and vertical planes. Indentation in the medial plane shows greater tissue relaxation than the other planes, indicating greater viscous flow under load. The greater relaxation shows decreased stiffness in the medial plane when compared to either the caudocephalic or vertical planes under indentation.

Discussion

The physical properties of cartilage have a great dependence on the structural organization of the extracellular components. In cartilage, the major components are collagen and proteoglycans. The amounts and organization of these components may vary substantially between different hyaline cartilages (Pietila and others, 1999). Articular cartilage has a depth-dependent anisotropic distribution of collagen (Xia, 1998), while cartilage from the nasal septum has commonly been considered to have a relatively homogeneous collagen distribution due to the ^{23}Na and ^{2}H nucleus of NMR in septal cartilage presenting only a residual quadrupolar interaction (Shinar and others, 1993; Zheng and Xia, 2009a), thought to arise from a local rather than a macroscopic order. Knowledge of such anisotropies within nasal septal cartilage may be surgically relevant when considering cartilage graft transplantation. Malrotation of articular cartilage grafts, causing collagen misalignments between the graft and host, has been suggested to decrease transplant longevity (Bisson and others, 2005). The potential for collagen anisotropies within septal cartilage may also affect the graft-host relationship by potentially being a cause of graft resorption, one of the most common failures of septal graft transplantation (Grellmann and others, 2006).

The current study has found remarkable consistency in the structural anisotropies in septal cartilage among three different methods, μMRI, PLM, and mechanical indentation. The T_2 findings from the μMRI experiments where specimens were rotated at angles between 0° and 180° showed considerable collagen anisotropy among the rotations of samples oriented in the vertical and caudocephalic planes (Fig 3). In contrast, the identical μMRI experiments showed nearly no change in T_2 from the samples oriented in the medial plane. Based on the understanding that the dynamics of the water protons in connective tissues is modulated by T_2 anisotropy hence sensitive to the fibril orientation in cartilage (Henkelman and others, 1994; Xia, 1998; Xia and others, 2001), the μMRI results clearly indicate that the long axis of collagen is oriented in parallel with the medial (y) direction (Fig 1).

The PLM results affirm the μMRI observation from a different physical mechanism, optical birefringence. Both the angle and retardation images in the vertical and caudocephalic planes show the long axis of collagen fibers, while images of samples in the medial plane show the short axis of the collagen fibers (Figs 4 and 5). The fact that the angle anisotropy in the vertical plane is nearly identical to that in the caudocephalic plane reflects the starting orientation of the tissue sections on the microscope stage to be approximately the same (c.f., Fig 4). Since the fibrils were oriented along the medial (y) direction, the samples sectioned in the medial plane contained the cross sections of collagen fibrils. However, small deviations from a perfect fibril bundle (evidenced by the wavy/zigzag nature of the fibrils) are unavoidable (Broom and Silyn-Roberts, 1989; de Campos Vidal, 2003), which will result in a finite residual angle, and consequently, an angle anisotropy when one rotates the medial section under PLM.

These observations from both μMRI and PLM imaging experiments are further supported by the mechanical indentation results that show decreased stiffness when nasal cartilage is

compressed in the medial plane when compared to indentation in either the vertical or caudocephalic planes (Fig 6), confirming a previous observation on compressing human nasal cartilage by Richmon *et al* (Richmon and others, 2006). The differences between imaging and compressing collagen fibrils either on their end or along their long axis may be analogous to the anisotropic differences seen in articular cartilage between the superficial zone (long axis of collagen oriented parallel to the articular surface) and the deep zone (long axis of collagen oriented perpendicular to the articular surface) (Xia and others, 2001; Zheng and Xia, 2009c). Previous studies into the depth-dependent anisotropies of articular cartilage have found differences between the superficial and deep zones using μMRI (the laminar appearance of articular cartilage in MRI) (Xia, 1998), PLM (the depth dependent profiles of fibril orientation and fibril organization) (Xia and others, 2001), and mechanical compression (the depth dependent stiffness which increases with increasing depth from the surface) (Chen and others, 2001a; Chen and others, 2001b). The present results show similar trends in septal cartilage and may indicate that the structure of the collagen matrix in septal cartilage may be analogous to the collagen orientation within the deep (radial) zone of articular cartilage.

Conclusion

In conclusion, this project shows that the collagen orientation in bovine nasal cartilage is not isotropic, where the long axis of collagen is found to be oriented in parallel with the medial direction in the tissue. The existence of such anisotropy in nasal cartilage is detected by three different techniques, each with a unique physical mechanism (water mobility in μMRI, birefringence in PLM, and compressive resistance in mechanical indentation). This anisotropy bears critical relevance to researchers using septal cartilage as a substitute for articular cartilage in NMR/MRI experiments as the T_2 value is closely related to the relative direction of collagens with respect to the direction of the static magnetic field. Additionally, these findings may have important clinical implications where collagen misalignment in cartilage grafts may hinder the long-term success of the transplant.

Acknowledgments

Y Xia is supported by the R01 grants (AR 45172, AR 52353) from the National Institutes of Health. The authors are indebted to C. Roy Inc. (Yale, MI) for providing the cartilage specimens, Dr. Aruna Bidthanapally for preliminary PLM work and critical discussions, and Mr. Farid Badar for assistance in specimen harvesting.

References

Arokoski J, Kiviranta I, Jurvelin J, Tammi M, Helminen HJ. Long-distance running causes site-dependent decrease of cartilage glycosaminoglycan content in the knee joints of beagle dogs. Arthritis Rheum. 1993; 36:1451–9. [PubMed: 7692860]

Bisson L, Brahmabhatt V, Marzo J. Split-line orientation of the talar dome articular cartilage. Arthroscopy. 2005; 21:570–3. [PubMed: 15891723]

Broom ND, Silyn-Roberts H. The three-dimensional 'knit' of collagen fibrils in articular cartilage. Connect Tissue Res. 1989; 23:75–88. [PubMed: 2632144]

Cardenas-Camarena L, Gomez RB, Guerrero MT, Solis M, Guerrerosantos J. Cartilaginous behavior in nasal surgery: a comparative observational study. Ann Plast Surg. 1998; 40:34–8. [PubMed: 9464693]

Chen A, Bae W, Schinagl R, Sah R. Depth- and Strain-dependent mechanical and electromechanical properties of full-thickness bovine articular cartilage in confined compression. J Biomechanics. 2001a; 34:1–12.

Chen SS, Falcovitz YH, Schneiderman R, Maroudas A, Sah RL. Depth-dependent compressive properties of normal aged human femoral head articular cartilage: relationship to fixed charge density. Osteoarthritis Cartilage. 2001b; 9:561–9. [PubMed: 11520170]

de Campos Vidal B. Image analysis of tendon helical superstructure using interference and polarized light microscopy. Micron. 2003; 34:423–32. [PubMed: 14680929]

Donald PJ. Cartilage grafting in facial reconstruction with special consideration of irradiated grafts. Laryngoscope. 1986; 96:786–807. [PubMed: 3523085]

Glasgold MJ, Kato YP, Christiansen D, Hauge JA, Glasgold AI, Silver FH. Mechanical properties of septal cartilage homografts. Otolaryngol Head Neck Surg. 1988; 99:374–9. [PubMed: 3148886]

Grellmann W, Berghaus A, Haberland EJ, Jamali Y, Holweg K, Reincke K, Bierogel C. Determination of strength and deformation behavior of human cartilage for the definition of significant parameters. J Biomed Mater Res A. 2006; 78:168–74. [PubMed: 16628548]

Henkelman RM, Stanisz GJ, Kim JK, Bronskill MJ. Anisotropy of NMR properties of tissues. Magn Reson Med. 1994; 32:592–601. [PubMed: 7808260]

Jeffery AK, Blunn GW, Archer CW, Bentley G. Three-dimensional collagen architecture in bovine articular cartilage. J Bone Joint Surgery. 1991; 73 B:795–801.

Jelicks LA, Paul PK, O'Byrne E, Gupta RK. Hydrogen-1, Sodium-23, and Carbon-13 MR spectroscopy of cartilage degradation in vitro. J Magn Reson Imaging. 1993; 3:565–568. [PubMed: 8347947]

Maas CS, Monhian N, Shah SB. Implants in rhinoplasty. Facial Plast Surg. 1998; 13(4):279–90. [PubMed: 9656882]

Muir H, Bullough P, Maroudas A. The distribution of collagen in human articular cartilage with some of its physiological implications. J Bone Joint Surgery. 1970; 52 B:554–563.

Pietila K, Kantomaa T, Pirttiniemi P, Poikela A. Comparison of amounts and properties of collagen and proteoglycans in condylar, costal and nasal cartilages. Cells Tissues Organs. 1999; 164:30–6. [PubMed: 10940671]

Reiter DA, Lin PC, Fishbein KW, Spencer RG. Multicomponent T(2) relaxation analysis in cartilage. Magn Reson Med. 2009; 61:803–809. [PubMed: 19189393]

Richmon JD, Sage A, Van Wong W, Chen AC, Sah RL, Watson D. Compressive biomechanical properties of human nasal septal cartilage. Am J Rhinol. 2006; 20:496–501. [PubMed: 17063745]

Rotter N, Tobias G, Lebl M, Roy AK, Hansen MC, Vacanti CA, Bonassar LJ. Age-related changes in the composition and mechanical properties of human nasal cartilage. Arch Biochem Biophys. 2002; 403:132–40. [PubMed: 12061810]

Shinar H, Knubovets T, Eliav U, Navon G. Sodium interaction with ordered structures in mammalian red blood cells detected by Na-23 double quantum NMR. Biophys J. 1993; 64:1273–9. [PubMed: 8494983]

Xia Y. Relaxation Anisotropy in Cartilage by NMR Microscopy (μMRI) at 14 μm Resolution. Magn Reson Med. 1998; 39:941–949. [PubMed: 9621918]

Xia Y. Averaged and Depth-Dependent Anisotropy of Articular Cartilage by Microscopic Imaging. Semin Arthritis Rheum. 2008; 37:317–327. [PubMed: 17888496]

Xia Y, Moody J, Alhadlaq H. Orientational dependence of T2 relaxation in articular cartilage: A microscopic MRI (μMRI) study. Magn Reson Med. 2002; 48:460–469. [PubMed: 12210910]

Xia Y, Moody J, Alhadlaq H, Hu JN. Imaging the Physical and Morphological Properties of a Multi-Zone Young Articular Cartilage at Microscopic Resolution. J Magn Reson Imaging. 2003; 17:365–374. [PubMed: 12594728]

Xia Y, Moody J, Burton-Wurster N, Lust G. Quantitative In Situ Correlation Between Microscopic MRI and Polarized Light Microscopy Studies of Articular Cartilage. Osteoarthritis Cartilage. 2001; 9:393–406. [PubMed: 11467887]

Xia Y, Ramakrishnan N, Bidthanapally A. The depth-dependent anisotropy of articular cartilage by Fourier-transform infrared imaging (FTIRI). Osteoarthritis Cartilage. 2007; 15:780–788. [PubMed: 17317225]

Xia Y, Zheng S, Bidthanapally A. Depth-dependent Profiles of Glycosaminoglycans in Articular Cartilage by μMRI and Histochemistry. J Magn Reson Imaging. 2008; 28:151–157. [PubMed: 18581328]

Zheng S, Xia Y. Effect of phosphate electrolyte buffer on the dynamics of water in tendon and cartilage. NMR Biomed. 2009a; 22:158–164. [PubMed: 18720450]

Zheng S, Xia Y. Multi-components of T2 relaxation in ex vivo cartilage and tendon. J Magn Reson. 2009b; 198:188–196. [PubMed: 19269868]

Zheng S, Xia Y. The collagen fibril structure in the superficial zone of articular cartilage by μMRI. Osteoarthritis Cartilage. 2009c; 17:1519–1528. [PubMed: 19527808]

Zheng S, Xia Y. On the measurement of multi-component T(2) relaxation in cartilage by MR spectroscopy and imaging. Magn Reson Imaging. 2010a; 28:537–545. [PubMed: 20061115]

Zheng S, Xia Y. The impact of the relaxivity definition on the quantitative measurement of glycosaminoglycans in cartilage by the MRI dGEMRIC method. Magn Reson Med. 2010b; 63:25–32. [PubMed: 19918900]

Zheng S, Xia Y, Badar F. Further studies on the anisotropic distribution of collagen in articular cartilage by muMRI. Magn Reson Med. 2011 in press.

Zheng S, Xia Y, Bidthanapally A, Badar F, Ilsar I, Duvoisin N. Damages to the extracellular matrix in articular cartilage due to cryopreservation by microscopic magnetic resonance imaging and biochemistry. Magn Reson Imaging. 2009; 27:648–655. [PubMed: 19106023]

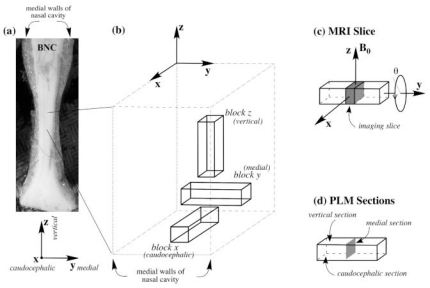

Fig 1.

(a) The anterior view of bovine septal cartilage, oriented in anatomical position. (b) An enlarged view of the tissue blocks used in the experiments showing their orthogonal directions and how they relate to the original tissue. (c) The location of the MRI slice, which was always the medial section through the middle of the long tissue block. θ refers to the orientation of the tissue block in the magnet. (d) The locations of the PLM sections.

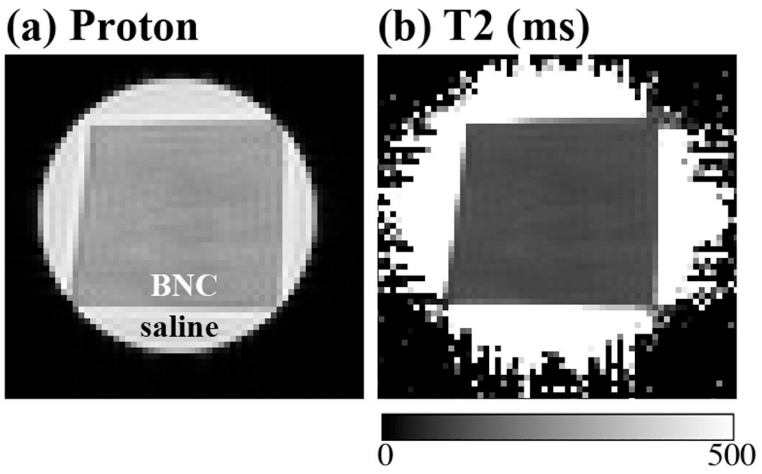

Fig 2.
(a) The μMRI proton image of a septal cartilage in the medial plane. (b) The T2 image (in ms) that was calculated from a set of proton intensity images.

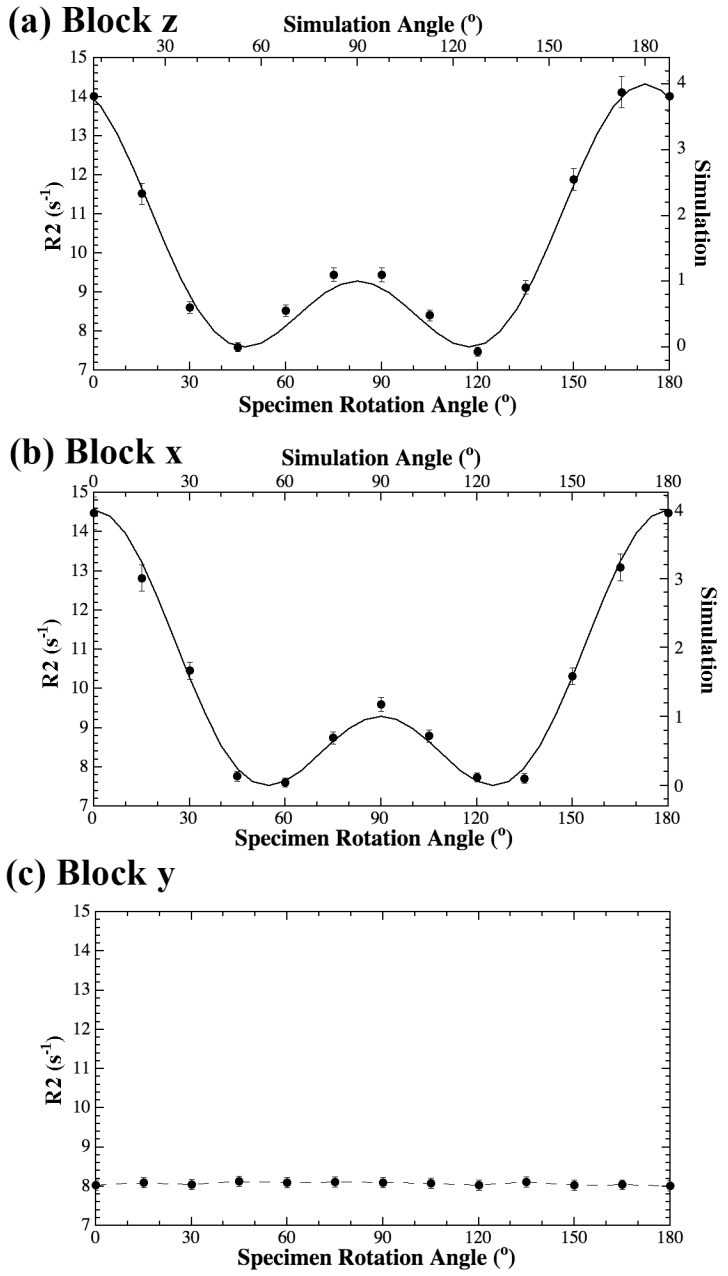

Fig 3.
The R2 (1/T2) anisotropy profiles for Block Z (a), Block X (b), and Block Y (c).

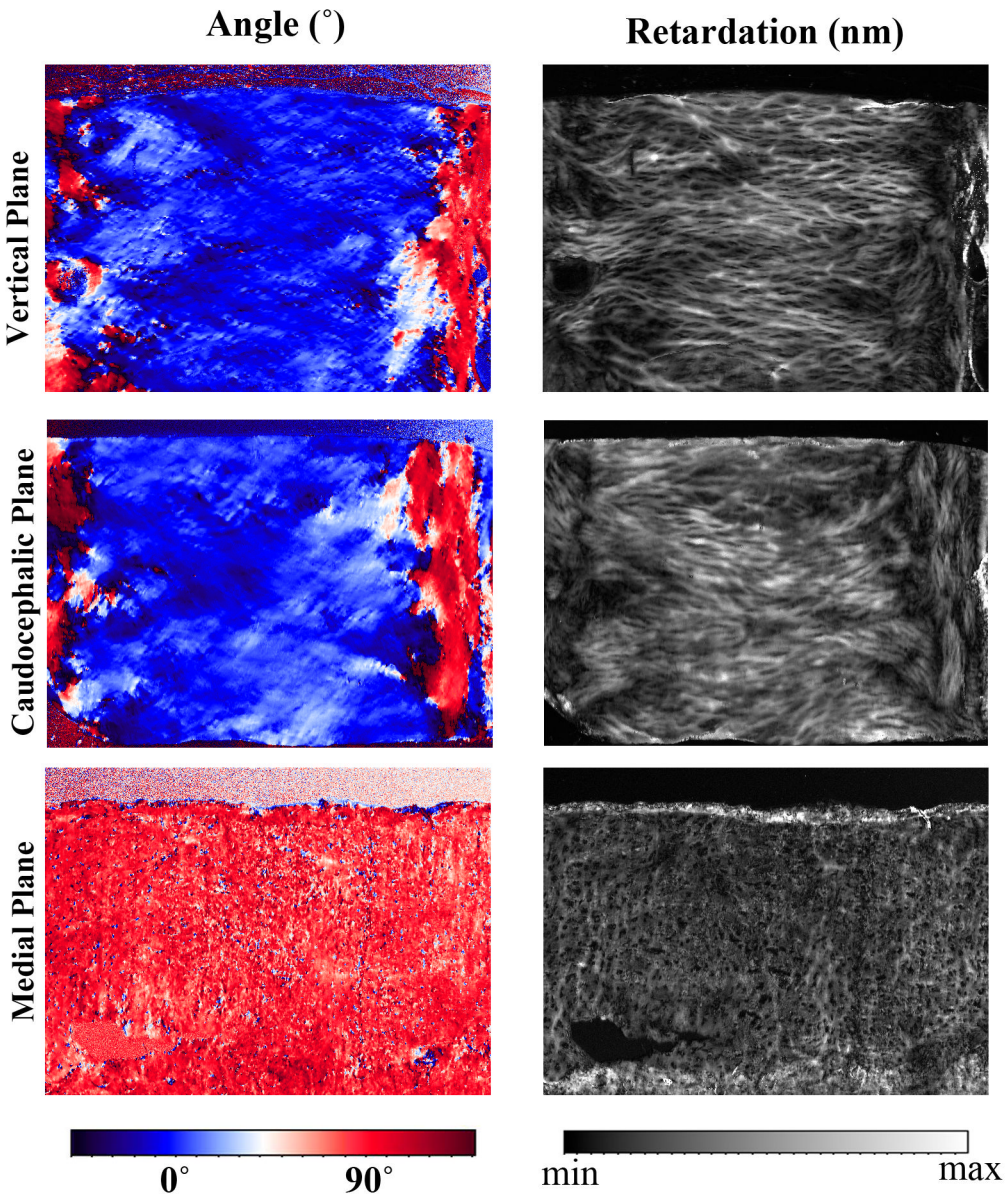

Fig 4.

The PLM angle (left column) and retardation (right column) images from the samples sectioned in the vertical, caudocephalic, and medial planes. In the angle images, the color blue and color red represent a 90° angle difference. In the angle images of the vertical and caudocephalic sections, the blue corresponds with the septal cartilage and the red corresponds with the mucosal walls of the interior of the nasal cavity.

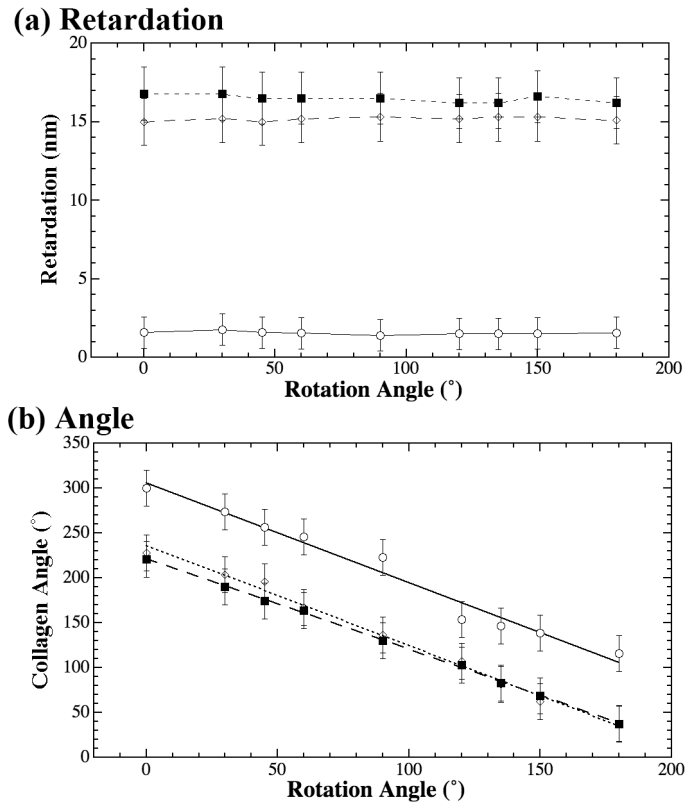

Fig 5.

The PLM angle and retardation profiles as a function of the specimen rotation, where the open circles, solid squares, and open diamonds were data points from samples sectioned in the medial plane, vertical plane, and caudocephalic plane respectively.

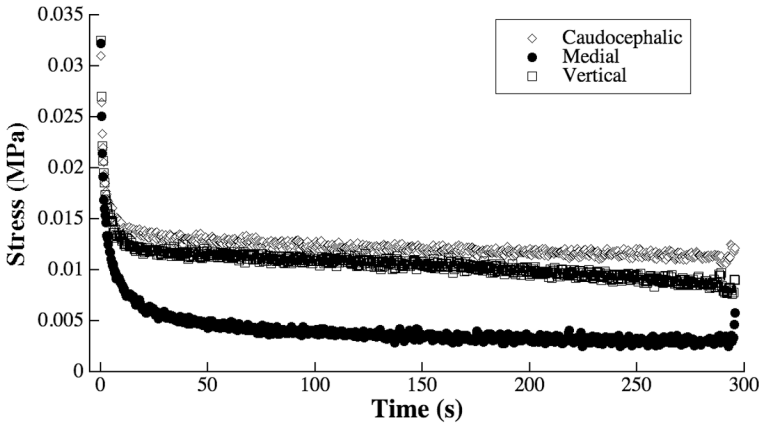

Fig 6.

The stress relaxation profiles of the three septal cartilage planes under indentation. Each line was averaged over all 11 specimens. Standard deviations (~0.01 MPa) were excluded to better illustrate the differences between the loading in the different planes.